Dimi-Misic, Katarina; Phiri, Josphat; Nieminen, Kaarlo; Maloney, Thad; Gane, Patrick

Characterising exfoliated few-layer graphene interactions in co-processed nanofibrillated cellulose suspension via water retention and dispersion rheology

Published in:
Materials Science and Engineering B: Solid-State Materials for Advanced Technology

DOI:
10.1016/j.mseb.2019.03.001

Published: 01/03/2019

Document Version
Peer-reviewed accepted author manuscript, also known as Final accepted manuscript or Post-print

Characterising exfoliated few-layer graphene interactions in co-processed nanofibrillated cellulose suspension via water retention and dispersion rheology

Katarina Dimi-Misic[1], Josphat Phiri[1], Kaarlo Nieminen[1], Thad Maloney[1] and Patrick Gane[1,2]

[1]Aalto University, Department of Bioproducts and Biosystems, School of Chemical Engineering, FI-00076 Aalto, Helsinki, Finland

[2] Omya International AG, Baslerstrasse 42, CH-4665 Oftringen, Switzerland

ABSTRACT

Few-layer graphene has been produced by mechanical delamination of exfoliated and naturally obtained graphite in aqueous suspension using the dispersion and suspension properties of nanofibrillated cellulose [NFC]. Various degrees of graphene platelet integrity were obtained depending upon the processing conditions and the optional adoption of surfactant to aid dispersion of the hydrophobic agglomerates of nanometre-thin carbon material. The presence of NFC in the suspension acts similarly to the presence of surfactant, increasing the hydrodynamic coupling between the particles and water as a function of processing time, regardless of the graphene-comprising source. In the light of extensive dynamic and viscoelastic rheological analysis, it was found that by fitting the stress growth region in the stress-shear rate relation to a concatenated series of single exponential functions of shear rate, the power law exponent and suspension consistency parameters [n and k] within a shear rate-localised Herschel-Bulkley [HB] expression provide a straightforward characteristic for monitoring the desired coupling response, and hence desired product constancy.

Keywords: few-layer graphene, micro/nanofibrillar cellulose, coprocessing graphite delamination in cellulose, graphene-cellulose-water interaction under flow, quality parameterisation, power law shear response

1. INTRODUCTION

Renewable and biodegradable cellulose based materials have shown promise for various potential applications including replacement of fossil oil-based materials due to their excellent functional properties [1, 2]. Cellulose fibres, which contain the most abundant natural polymer, can be processed to form microfibrillated cellulose (MFC) or nanofibrillated cellulose (NFC) by mechanical, chemical or enzymatic processes [3, 4]. NFC has been demonstrated in many applications related to its functional properties such as high surface area, high strength, biodegradability, low density etc. [1, 4, 5]. The nanofibrils in NFC are typically 4-20 nm nanometres in diameter and a 500 – 2 000 nm in length [6]. When dispersed in water, these highly surface charged fibrils form a stable dispersed transparent gel-like suspension, at concentrations as low as 0.03 % via hydrogen bonding between nanofibrils and water molecules [7, 8]. Due to the high aspect ratio and easily modifiable surface chemistry, MNFC has high potential to act as a building block for various applications including reinforcement in polymer matrices, aerogels, foams, nanopaper, transparent and flexible films [9]. Chemical pre-treatments of pulp significantly lower the energy consumption in NFC production, making the industrial manufacture of NFC economically feasible [1, 2, 10]. One such treatment is aqueous (2,2,6,6-tetramethylpiperidin-1-yl)oxyl (TEMPO)-mediated oxidation, due to its high efficiency and moderate chemical costs [7]. TEMPO-mediated oxidation that drastically reduces the energy consumption during the

pulp disintegration to NFC through enabling breakdown of the fibre structure into the nanofibrillar form with high surface charge, which, due to the high aspect ratio of the fibrils, acts as a water binding agent and provides strong repellance between the particles, resulting in the formation of the gel, which in the case of pure nanofibrils is transparent [10, 12].

Graphene, on the other hand is a 2-dimensional material that has attracted a lot of attention due to its fascinatingly unique properties [15, 16]. Single graphene sheets have shown extremely high values of electron mobility > 200 000 $cm^2V^{-1}s^{-1}$ at room temperature, which are much greater than in metals or even semiconductors [16, 17]. Graphene is also ~200 times stronger than steel with a Young's modulus of 1 100 GPa and fracture strength of about 125 GPa [17, 18]. Theoretically, graphene has a specific surface area of 2 630 m^2g^{-1} and extremely high thermal conductivity of 5 000 $Wm^{-1}K^{-1}$, which is greater than that of diamond [20]. Apart from generating mechanical properties, graphene's extraordinary electrical properties will direct its utilisation as a filler in many composites designed to act as super capacitors [21, 22]. These properties of graphene have led to a wide range of potential applications including printable electronics, nanocomposites, sensors , printable solar cells , transparent electrodes and catalysts [23-31]. However, large-scale application of graphene is still a major challenge due to lack of feasible, viable and efficient production methods [32, 33].

Fabrication of electrically conductive and mechanically strong graphene-based composites, especially those including biodegradable and renewable polymers, is of significant interest [35, 41]. One of the major potential and promising applications of graphene is its use as a functional reinforcing filler in the production of composite materials [29, 31]. One such example is graphene-NFC nanocomposite, which can have a variety of functional properties [33, 34, 35**]**. Additionally, strengthening could, for example, enhance the utilisation of NFC in many practical applications including gas barriers, and where reduced weight is important [9, 17, 23]. Furthermore, application of graphene in NFC composite papers has shown to add hydrophobic performance to an otherwise highly hydrophilic surface [18, 33, 36].

The majority reported work so far describes the production of graphene oxide [GO] or reduced graphene oxide [RGO], derivatives of graphene that are prepared by oxidation of graphite rather than by mechanical delamination [36]. Relative to the oxidised graphene oxide (GO) the reduced graphene oxide [RGO] has superior electrical conductivity [21, 25, 30] with oxygen containing groups on the surface providing pseudo-capacitive storage charge (via Faradaic reaction mechanism) in addition to its double layer storage. This promising material can be qualified for condensed-matter and high energy physics applications, as well as in material science, cellular imaging, drug delivery and biological material applications, together with a wide range of other technological applications such as bioelectronics and biosensing [26, 32, 36]. However, the strong tendency for RGO to agglomerate and re-stack can deteriorate overall electrical capacitance [18, 30].

Unfortunately, the fabrication methods for GO or RGO utilise toxic chemicals and processing conditions, which are not conducive to environmental protection and are challenging to implement in large scale production of graphene and its derivatives to reach the industry's increasing needs [18, 35]. Consequently, with graphene being potentially in contact with the environment, we should consider the environmental issue and the safety of these nanomaterials regardless their benefits. Thus, for the sustainable implementation of graphene, it is important to develop mechanical routes for its production, which can deliver pristine graphene, but which can offer utility in different composites [34, 36].

The reported studies of mechanical fabrication of pristine graphene generally involve liquid phase exfoliation of graphite in synthetic surfactant systems, which, if they remain on the surface of graphene particles, are not desirable for the onward production of composites [33]. The amphiphilic nature of cellulose fibres, however, enables them to act as both dispersing and homogenising agent prior to use in graphene-cellulose composite

suspensions [33, 35, 37, 38]. Such a direct exfoliation process potentially using NFC provides an environmentally friendly and more cost-effective alternative for the fabrication of graphene, and therefore it is important to understand the mechanism of hydrodynamic interactions between a graphene particle and thixotropic NFC suspension under transition to high strain under high speed/high pressure processing conditions [36]. Moreover, since pristine graphene has a tendency for agglomeration due to its surface chemistry, being partially hydrophobic and morphologically unique, the suspension exhibits a complex thixotropic nature similar in some respects to that of MNFC suspensions [32, 36]. Thus, for the successful production of graphene-NFC composites, it is important to understand and tune the set of mutual rheologically complex flow or strain conditions [37, 39]. Cellulose nanofibrils can act as surface active dispersant for graphite and ultimately graphene particles during refining including the potential for entering into the two dimensional layers of stacked graphene sheets and between individual particles within graphene agglomerates for improved hydrodynamic coupling to promote delamination during exfoliation [37, 38].

Given the different pre-treatments and production routes exfoliation of graphite it is not surprising that each combination results in a difference in morphology and polarity of the particles, which affect the level of repulsion or aggregational attraction between the graphene particles in native dispersion and in the NFC gel-like suspension matrix. Furthermore, NFC aqueous suspension is a non-Newtonian fluid, highly dependent on flow conditions, and the increase of shear rate enhances both the aggregation and fragmentation of the fibrillar colloid system, which results in flow behaviour which displays thixotropy with a final equilibrium state being dependent on parameters characteristic of the particles and their interactions [34, 39].

The present work applies the study of rheology as a tool to examine the influence of the pre-treatment and refining time and the behaviour of the graphene particles in the supporting NFC suspension in which the nanocellulose component is used as constituent dispersion and production aid. and constituent in NFC-graphene composite [36, 39, 40] The rheology of complex particulate gel-like suspensions is related initially to the mechanical aspects under the application of strain from the static state, such as extension and breaking of the particle-particle bonds and the distortion and collapse of the cage structure entrapping water in the gel matrix [41, 42]. Graphene-NFC composite suspensions will add complexity by incorporating both the flexible surface-surface bonds of the graphene aggregates and the fibrillar gellant particles interspersed with bound water [36]. Probing the composite suspension under carefully defined shear gradient is designed to reveal the dispersion properties of the graphene transitioning non-linearly from retained hydrophobic interactions of graphene, through the sought-after dispersion via NFC-graphene interaction enhancing wettability, followed by physical entanglement [44-46]. Coprocessing graphite with NFC suspension is studied also in search of synergy arising from the material codelaminating process. The action of graphene particles in respect to dewatering of NFC suspensions is to date largely unknown.

2. Materials and Methods

Deionised water was used throughout the experimentation.

2.1 Cellulose fibre raw material

Never dried laboratory bleached Kraft birch pulp [kappa number 0.96] was used as the raw material for the TEMPO-mediated (2,2,6,6-tetramethylpiperidin-1-yl)oxyl, (Sigma Aldrich (St Louis, USA)) oxidation to produce the NFC. In the reaction 13 % NaOCl solution (Merck (Darmstadt, Germany)) was the primary oxidant used.

2.2. NFC production

Definition of TEMPO mediation and the oxidation route. NFC-TEMPO suspension was made at 2.3 w/w% and diluted to 1.9 w/w% by mixing into water.

2.3. Surfactant solution

Sodium cholate (SC) surfactant was purchased from Sigma Aldrich and used as received without any modification. A surfactant solution was prepared by dissolving SC in water at a concentration of 3 $mgcm^{-3}$.

2.4. Graphite raw material for graphene production

Expanded graphite (EG) was provided by Asbury Carbon; natural graphite flakes (NGF) was purchased from Sigma Aldrich. NGF was used as received without any modifications.

2.5. Preparation of graphene suspensions

Thermal exfoliation was applied as a pre-treatment to EG by heating for ~20 s in a muffle oven at 700 °C before being mixed with the respective chosen media [36].

NGF and EG graphite suspensions were prepared at a concentration of 8 $mgcm^{-3}$ in three different media: water (W), surfactant solution (S) and NFC aqueous suspension (NFC). 500 cm^3 of each prepared suspension was subjected to shear exfoliation performed using an IKA Magic Lab ([1-*l* Module MICRO-PLANT equipped with a single walled open 1 dm^3 vessel) high shear mixing equipment with a maximum flow rate of 80 dm^3h^{-1} at a rotation speed of 20 000 min^{-1} (rpm) for a predetermined time. 100 cm^3 sample aliquots were collected after 15, 30, 60, 90, 120 min for analysis as shown in Fig. 1.

The exfoliation refining, R, described above, is referred to in terms of the medium used and the material being exfoliated $R^{medium}{}_{material}$, e.g. NGF exfoliated in the process with water, W, as the medium is given the label $R^{W}{}_{NGF}$ etc.

As controls, direct mixes with separately processed NFC were made of each material post processing in water, i.e. aqueous suspensions of NGF and EG processed alone, namely $R^{W}{}_{NGF}$ and $R^{W}{}_{EG}$ mixed with separately processed NFC suspension. The refining in each case of mixing post processing ($R^{W}{}_{material\ 1} + R^{W}{}_{material\ 2}$) is referred to as $R^{W}{}_{NFC\ +\ material\ 2}$, i.e. $R^{W}{}_{NFC\ +\ NGF}$ and $R^{W}{}_{NFC\ +\ EG}$, respectively.

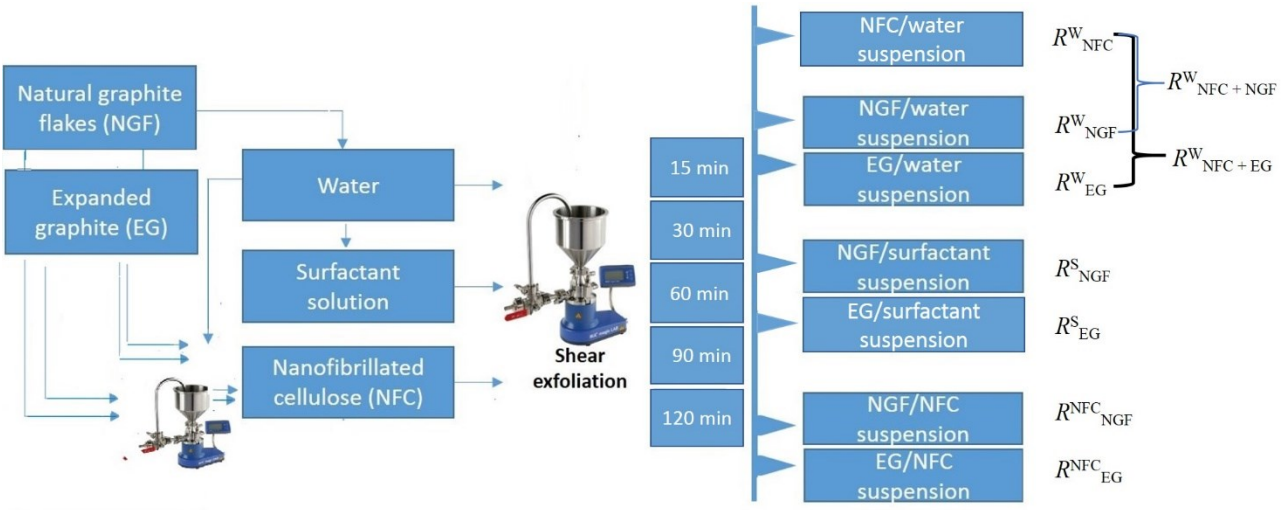

Fig. 1 Schematic representation of graphene exfoliation from either natural graphite flakes (NGF) or expanded graphite (EG) in water, surfactant and two ways of refining in combination with NFC suspension, respectively.

Table 1 Suspensions of graphene and graphene/NFC suspensions used in this research, produced as presented in the Fig. 1.

Exfoliated refined suspension *Refining time*: 15/30/60/90/120 min	**Material in aqueous suspension**	**Process suspension medium**
R^{W}_{NGF}	Natural graphite flakes [NGF]	Water (W)
R^{W}_{EG}	Expanded graphite [EG]	
R^{W}_{NFC}	Nanofibrillated cellulose [NFC]	
R^{S}_{NGF}	Natural graphite flakes [NGF]	SC surfactant solution (S)
R^{S}_{EG}	Expanded graphite [EG]	
R^{NFC}_{NGF}	Natural graphite flakes [NGF]	NFC suspension (NFC)
R^{NFC}_{EG}	Expanded graphene [EG]	
$R^{W}_{NFC + NGF} = [R^{W}_{NFC} + R^{W}_{NGF}]$	Nanofibrillated cellulose + Natural graphite flakes [NFC + NGF] *mixed after separate processing*	Water (W)
$R^{W}_{NFC + EG} = [R^{W}_{NFC} + R^{W}_{EG}]$	Nanofibrillated cellulose + Expanded graphite [NFC + EG] *mixed after separate processing*	

2.6 Gravimetric dewatering/ water retention (ÅA-GWR)

The static gravimetric dewatering of the suspensions was measured using the Åbo Akademi Gravimetric Water Retention device (ÅA-GWR), as described in detail in our previous publications [8, 11]. A volume of 5 cm^3 of suspension was inserted into the cylindrical vessel above a polycarbonate membrane (Nucleopore Track-Etch membrane 0.5 μm (Whatman)) and a stack of absorbent blotter papers. The cylinder was closed, and the sample held under an overpressure by applying a vacuum beneath the apparatus, $|-\Delta p| = 50$ kPa for 90 s, during which time dewatering through the membrane occurred. The blotter paper sheet/stack was weighed before the start of the dewatering measurement and after when the pressure was released. The weight difference was multiplied by 15 091 m^{-2}, which is the inverse of the cylinder cross-sectional area. An average of five determinations was computed.

2.7 Rheology

2.7.1 Shear response

Shear flow measurements were used for the determination of dynamic viscosity (η) performed with bob in cup geometry, where the "bob" was a four-bladed vane spindle with a diameter of 10 mm and a length of 8.8 mm, while the metal cup had a diameter of 17 mm (Anton Paar, Germany) [43,]. Flow curves of the NFC gel-like suspension were measured as a function of decreasing shear rate, spanning a wide shear rate range ($\dot{\gamma}$= 1 000 – 0.01 s^{-1}) with a logarithmic spread of data point collection duration, ranging from 1 to 100 s [62, 63].

The Ostwald-de Waele expression for the purely viscous shear thinning [8, 11] is given by

$$\eta = k\dot{\gamma}^{n-1} \tag{1}$$

and used to fit the thixotropic shear response behaviour, where k and n in Eq. 1 are the consistency and power law index, respectively, and $\dot{\gamma}$ is the shear rate.

2.7.2 Viscoelastic response

For the oscillatory viscoelastic measurements plate-plate geometry with serrated surface profile on both upper and lower plates was used to avoid apparent wall-slip due to sample depletion. The upper plate diameter was 20 mm and gap setting of 2.3 mm. The bottom plate was connected to a Peltier block temperature control, set to a constant temperature of 23 ˚C. All suspensions were measured five times and for each measurement a new sample was used [47].

Prior to the oscillatory measurements, the samples were pre-sheared at a shear rate of $\dot{\gamma}$ = 100 s^{-1} for 60 s and then left to rest for another 60 s [49-51]. Each oscillatory measurement then started with an amplitude sweep, applying strain [γ] across the range between 0.1 and 500 % maintaining a constant angular frequency (ω) of 10 [rad]s^{-1}, to determine the effective linear viscoelastic region (LVE) [53, 62]. For the following corresponding frequency sweep measurement, a constant strain of γ = 0.1 % in the LVE region was applied whilst angular frequency (ω) spanned the range of 0.01-100 (rad)s^{-1}. The dynamic moduli, storage modulus (G') and loss modulus (G''), were followed as a function of strain amplitude (γ) and span of angular frequency (ω). The influence of increase in angular frequency (ω) on the complex viscosity (η^*) was evaluated by measuring its response as a function of increasing angular frequency (ω = 0.1-100 (rad) s^{-1}).

To define differences between the respective suspensions regarding their colloidal interactions, packing effects and friction between graphene particles and/or nanofibrils during the flow, log-log plot flow curves of the

complex viscosity (η^*) were also fitted to a power law according to an equivalent for of the Ostwald-de Waele empirical model, Eq. 3, allowing for the comparison of different water binding properties within the linear viscoelastic region (LVE) for an effective complex viscosity (η^*), using an effective shear rate determined as the root mean square value under oscillation, and effective dynamic viscosity beyond the elastic region (η), respectively [51, 52]

$$A(t) = A_0 \sin\omega t$$

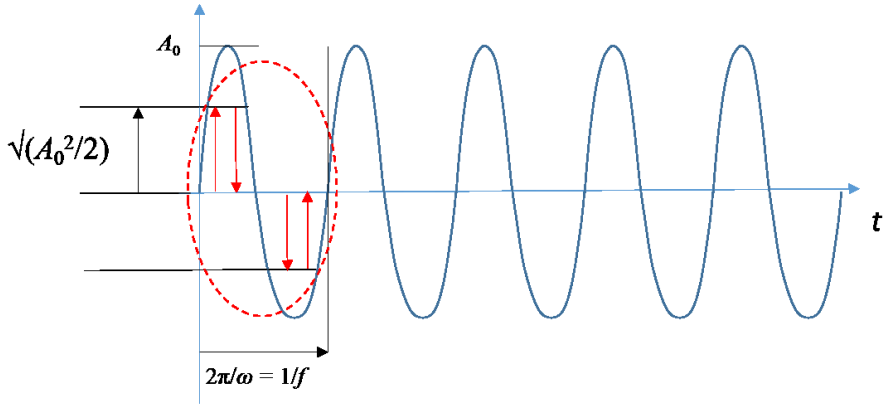

root mean square velocity $= v_{rms} = (\omega/2\pi).4\sqrt{(A_0^2/2)} = (\omega/\pi).2(A_0/\sqrt{2}) = (\omega/\pi).A_0\sqrt{2}$

$\Rightarrow$ shear rate, $v_{rms}/A_0 = d\gamma/dt = (\omega/\pi).A_0\sqrt{2}/A_0 = \sqrt{2}(\omega/\pi)$

Fig. 2 Derivation of the rms shear rate from a sinusoidal oscillation.

For a sinusoidal oscillation with angular frequency ω, Fig. 2, the root mean square velocity is given by

$$v_{rms} = \frac{\sqrt{2}}{\pi}\omega A_0 \tag{2}$$

where A_0 is the amplitude of the oscillation. We can, therefore, derive a root mean square shear rate $\dot{\gamma} = v_{rms}/A_0$, such that the Ostwald-de Waele shear thinning model can be approximated in the case of complex viscosity as

$$\eta^* = k_c(\dot{\gamma}_{rms})^{n_c-1} = k_c\left(\frac{\sqrt{2}}{\pi}\omega\right)^{n_c-1} \tag{3}$$

where k_c and n_c in Eq. 3 are the flow consistency index and the power-law exponent, respectively, for the complex viscoelastic case: $n_c = n = 1$ indicates a Newtonian fluid, whereas $n < 1$ indicates a pseudo-plastic [shear thinning] behaviour.

2.7.3 Rheological data variation

Data variation in the rheological measurement for the gel-like thixotropic systems was within 10 %. Noise reduction in the raw data was additionally applied using Tikhonov regularisation [10, 13]. The first step in the correction process is to remove obvious outliers [negative values and values out of scale]. The actual Tikhonov regularisation step consists of minimising a linear combination of a residual term (between raw and smoothed data) and a term representing the amount of remaining noise in the smoothed data. Adjusting the ratio between the coefficients in the linear combination determines the level of smoothness of the smoothed data. Fitting low order polynomials to the ends of the data and replacing the y-coordinates of the ends with values calculated

from the fits prevents the appearance of unnecessary winding at the ends. If necessary, the smoothing procedure could be advanced segmentally.

2.7.4 Consecutive yield stress

Yield stress is perhaps the most important rheological property of complex suspensions, as it needs to be exceeded in order that they can flow, which is challenging to evaluate for such wall slip prone materials as NFC-containing suspensions, which display shear banding to minimise stress when sheared [8, 12, 42]. Therefore, we use both static yield stress, (τ_s^0) obtained from the LVE region conducted with plate-plate geometry, and dynamic yield stress (τ_d^0) from flow curves conducted from vane in cup geometry [14, 43]. The dynamic yield stress (τ_d^0) is defined as the minimum stress required for maintaining the flow, while static yield stress (τ_s^0) is defined as the stress required for initiating flow, and the latter often has the higher value for NFC suspensions [4, 10, 43].

The Herschel-Bulkley equation describes the presence of a dynamic yield stress (τ_d^0) from the plot of the flow curves as [48-50],

$$\tau_d = \tau_d^0 + k\dot{\gamma}^n \tag{4}$$

where the terms k and n are the consistency and flow index, respectively, as presented in Eq. 1, with, once again, the value of $n < 1$ describing a material exhibiting shear thinning, and $n = 1$ Newtonian behaviour.

As strain (γ) is constantly increased at constant frequency (ω) from oscillatory amplitude sweep measurements, the maximum in the elastic stress (τ_s) that corresponds to the static elastic yield stress (τ_s^0) is determined as the first point of deviation from linear elastic deformation occurring at a corresponding critical strain value (γ_c) [51, 52]. The elastic stress component in oscillatory mode is given by

$$\tau_s^0 = G'\gamma_c \tag{5}$$

2.7.5 Suspension structure recovery

Structure recovery measurements were performed with the three-interval thixotropy test (3ITT) using bob in cup geometry (55-57). In this test, the evolution of transient viscosity η^+ after high shear rate is found by applying a step-wise shear rate with three defined intervals of applied shear, namely a low shear interval/ high shear interval/ low shear interval procedure. During the first and third intervals, the sample is sheared at low shear rate, $\dot{\gamma} = 0.1\ s^{-1}$, and in the second interval at high shear rate, $\dot{\gamma} = 1\ 000\ s^{-1}$. Recovery behaviour is defined after the dilatant increase of transient viscosity η_t+ in third interval has been overcome it its maximum value, and recorded as the reduced values of η_t^+ / η_0, where η_0 is the viscosity value at the start-up of the first interval [13, 78].

2.8 Scanning electron microscopy (SEM)

To visualise the structure of the NFC-graphene composites and so provide a correlation with the observed rheological properties, images were recorded using a Zeiss Sigma VP scanning electron microscope at 1–2 kV acceleration voltage. The samples for SEM imaging were prepared by freeze-drying the suspensions, followed by sputtering with a ~4 nm platinum film.

2.9 Particle and agglomerate size in suspension

The particle size distributions of the water medium-processed and post-process mixed agglomerate structures were measured with a Mastersizer (Malvern Instruments, UK) and compared with the surfactant processed graphene product to illustrate the role of graphene dispersion in the process [9, 14]. Prior to measuring, the samples were diluted with de-ionised water to a solid content of 0.01 %. The scattering volume equivalent median diameter ($d_{sv}(50)$) is also reported as an average of at least five separate measurements . In the case where the density of a material is constant throughout its size distribution, the volume and weight determined size distribution are identical.

3. Results and Discussion

3.1 Water retention

Flocculation and/or agglomeration within the suspension particulate matrix results in particle clusters [79-81]. The finer the constituent particles, the greater is the water retention tendency for the case of hydrophilic surfaces [57-59] Thus, water retention is strongly dependent on process refining time and/or whether surfactant-acting material is present to ensure the hydrophilicity of the constituent graphene particle surfaces [36, 37]. Processing of graphite to few layer graphene in the presence of a stabiliser surfactant or hydrodynamic shear-coupling NFC is, therefore, seen to promote water retention, suggesting that the material is both finer and hydrophilic [36]. In addition, the NFC presence creates a gel-like structure which itself develops higher water retention [8, 10, 11]. However, if hydrophobic large graphene agglomerates are present, the water retention is greatly reduced. Thus, by studying the results shown in Table 2, the lowest quoted dewatering value [highest water retention] corresponds to the combination of the gel-like action of NFC combined with the highly refined graphene created by processing the graphite in a medium of NFC suspension $R^{NFC}{}_{NGF}$ and $R^{NFC}{}_{EG}$, and this despite the lower solids consistency of the NFC-containing samples. We can also extract from the data that the graphite material EG is developing finer structures that the NGF. Interestingly, and importantly, the water retention of the graphene materials formed from graphite coprocessed with NFC is greater than when graphene is formed from graphite processed in water alone is mixed post processing with separately processed NFC.

Table 2 Gravimetric water retention results (ÄA-GWR) for graphene suspensions and graphene-NFC complex suspensions, compared with processing in the presence of surfactant, as a function of refining time.

Refining time /min	**Gravimetric dewatering /gm^{-2}**							
	Graphene suspensions - consistency 4 w/w%				Graphene-NFC composite suspensions - consistency 2 w/w%			
	$R^{W}{}_{NGF}$	$R^{W}{}_{EG}$	$R^{S}{}_{NGF}$	$R^{S}{}_{EG}$	$R^{W}{}_{NFC+NGF}$	$R^{W}{}_{NFC+EG}$	$R^{NFC}{}_{NGF}$	$R^{NFC}{}_{EG}$
15	6 829	6 697	6 478	6 256	5 889	5 344	5 203	4 848
30	6 714	6 234	6 143	5 887	5 387	4 982	4 653	4 524
60	6 423	5 897	5 876	5 623	4 824	4 503	4 218	4 145
90	5 823	5 421	5 473	5 276	4 577	4 098	3 819	3 556
120	5 324	5 198	5 137	4 987	4 125	3 687	3 524	3 249

We can conclude, even at this early stage of the analysis, that there is a clear synergy in coprocessing graphite with NFC versus post process mixing. Furthermore, given the higher water retention achieved during coprocessing with NFC, it is likely that there is greater hydrodynamic coupling between the liquid phase and

the particles during the shearing action in the refiner. This, then, is the major hypothesis to be tested rheologically.

3.2 Rheological experiments

3.2.1 Graphene dispersions in water – action of surfactant

3.2.1.1 Dynamic shear

The steady state shear curves of graphene suspensions, Fig. 3, produced from graphite in water, and graphite in surfactant solution, reveal that the suspensions have shear thinning behaviour at low shear rate, and a slight tendency to transient dilatancy at higher shear rate [41, 43, 45, 48]. The Ostwald-de Waele expression (Eq. 1) can be fitted to the shear thinning low and medium shear region, thus providing characteristic fitting values for consistency coefficient *k* and power index *n*. Smaller *n* indicates greater shear thinning and larger *k* indicates higher static state viscosity, related to flocculation/agglomeration, and driven mainly by the hydrophobic nature of the graphene particles in water. Hence, when processing together with surfactant the consistency value *k* drops as the particles become at least partially stabilised. Dilatant behaviour at the high shear rate may be considered related to shear-induced aggregation as the weak stabilising force is overcome during forced close contact of the particles, leading to coalescence due to the attractive hydrophobic force [47, 48].

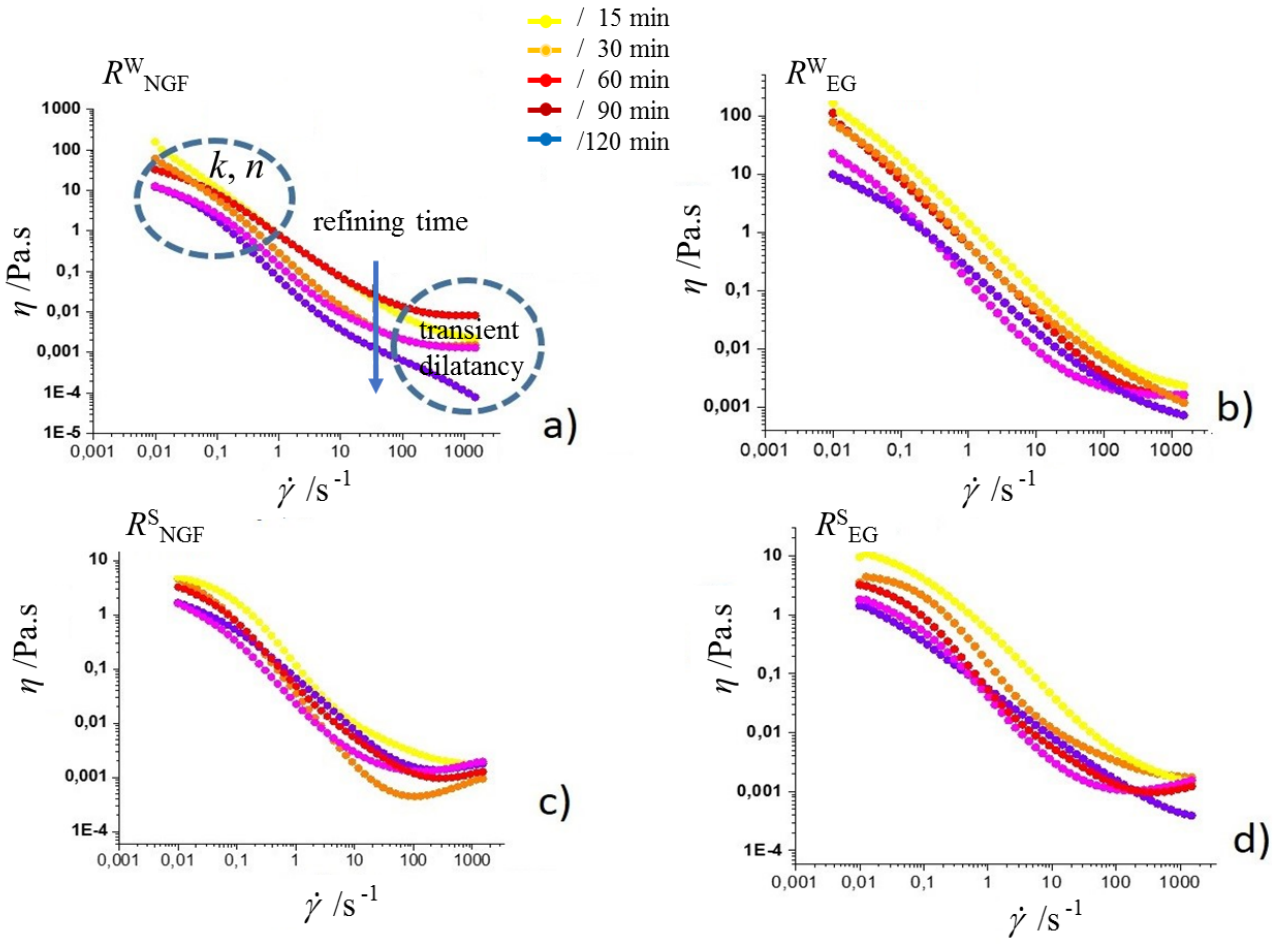

Fig. 3 Flow curves of graphene in water and surfactant suspension in response to refining time: (a) NGF processed in water, (b) EG processed in water, (c) NGF processed in surfactant solution, and (d) EG processed in surfactant solution. The effect of surfactant in reducing viscosity is clearly seen, though the tendency to shear induced aggregation for the surfactant containing system is relatively marked due to the mechanism of close encounter overcoming the weak stabilisation.

The values of consistency coefficient *k* and power index *n* are shown in Table 3. Both *k* and *n* decrease as a function of refining time and further on using surfactant in the refining fluid medium.

Table 3 Dynamic viscosity (η) rheological parameters according to the Ostwald-de Waele shear thinning power law.

Refining time /min	***k* consistency coefficient /Pa.s^n**				***n* < 1 shear thinning**			
	R^{W}_{NGF}	R^{W}_{EG}	R^{S}_{NGF}	R^{S}_{EG}	R^{W}_{NGF}	R^{W}_{EG}	R^{S}_{NGF}	R^{S}_{EG}
15	2.63	2.24	1.94	1.61	0.21	0.16	0.12	0.09
30	2.17	1.94	1.64	1.44	0.16	0.14	0.09	0.08
60	1.85	1.71	1.31	1.16	0.14	0.12	0.08	0.06
90	1.43	1.33	1.22	1.11	0.11	0.10	0.07	0.06
120	1.28	1.18	1.14	1.09	0.09	0.08	0.06	0.03

3.2.1.2 Dynamic yield stress

Extrapolating the sheared material stress curve back to the limit of zero shear, $\lim_{\dot{\gamma}\to 0} \tau_d^{\,0} = \eta\dot{\gamma}$, provides the value of stress required just to keep the suspension flowing, termed the dynamic yield stress $(\tau_d^{\,0})$ [58, 59]. This is a measure of the flocculation tendency in the particulate dispersion. As can clearly be seen, as expected, the use of surfactant increases the flowability of the dispersion by acting against flocculation, and the refining energy input [time] also breaks down the graphite into graphene platelets which tend to form looser structures in the static state.

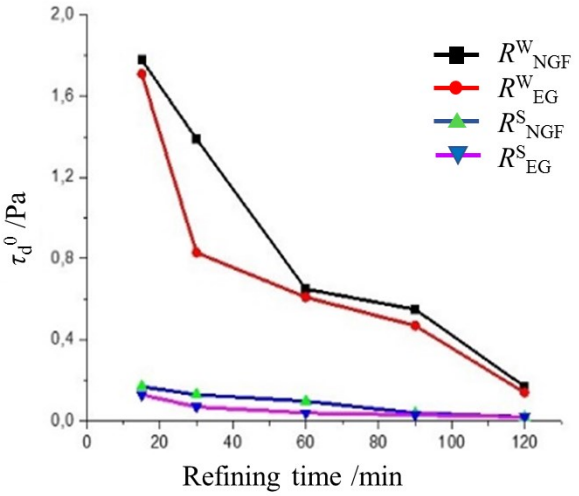

Fig. 4 Comparing the dynamic yield stress (τ_d^0) for graphene produced in water and graphene produced in surfactant solution as a function of refining time.

3.2.2 Graphene-NFC composite suspensions

Since the dynamic shear viscosity properties of graphene-NFC composite suspensions are dominated by the water-holding gel-like and strongly shear thinning behaviour of NFC, and so the graphene-graphene interactions tend to be hidden, it is decided here to present and compare the viscoelastic, and yield stress, response to strain amplitude and frequency, and shear, applied respectively, to the product composites [4, 10, 11].

3.2.2.1 Viscoelastic analysis

The strain applied to the suspensions ranges γ = 0.01–500 % using parallel plate geometry. As strain increases we see that the elastic response follows two structural modes, as shown by the two arrows in Fig. 5. Firstly, a weaker static loose floc/agglomeration structure, included in the NFC gel-like matrix, yields and then the system retains a stronger particle-particle aggregation interaction until the strain is sufficient, secondly, to break this down into a more purely viscous state [8, 42]. The decoupling of the weaker first stage floc behaviour followed by the particle-particle aggregation structure reveals an interesting trend in respect to refining time, in that the refining leads to big differences in respect to the weaker floc structure, but less so in respect to the particle-particle aggregation [32, 41, 43].Notable is the fact that the behaviour of the viscoelastic response is similar whether the graphite has been coprocessed with NFC ($R^{NFC}{}_{NGF}$ and $R^{NFC}{}_{EG}$) or the separately processed NFC has simply been added to the water processed graphite ($R^{W}{}_{NFC+NGF}$ and $R^{W}{}_{NFC+EG}$). This tells us that the weakening of the floc structure, as we saw earlier linked with increasing water retention, is dependent on the particle number and hydrophilicity. The longer the refining time, the greater the number of material particles that are generated, and the particle size is reduced [38]. Therefore, the larger scale loose floc structure associated with coarse particles decreases but the stronger particle-particle aggregation is retained.

To aid comparison of the magnitude of the viscoelastic response, moduli values at two strain levels are shown in Table 4. The strain levels are chosen to reflect the two-stage structure regime, i.e. at γ = 0.01 % and γ = 1.12 %, Fig. 5, to indicate the separation of agglomerated graphene particles from the gel-like loose floc within the NFC matrix at very low strain, and their subsequent mixing together with the NFC fibrils at higher strain within the second stage linear viscoelastic region LVE, before reaching critical strain γ_c, at which the elastic moduli drastically decrease.

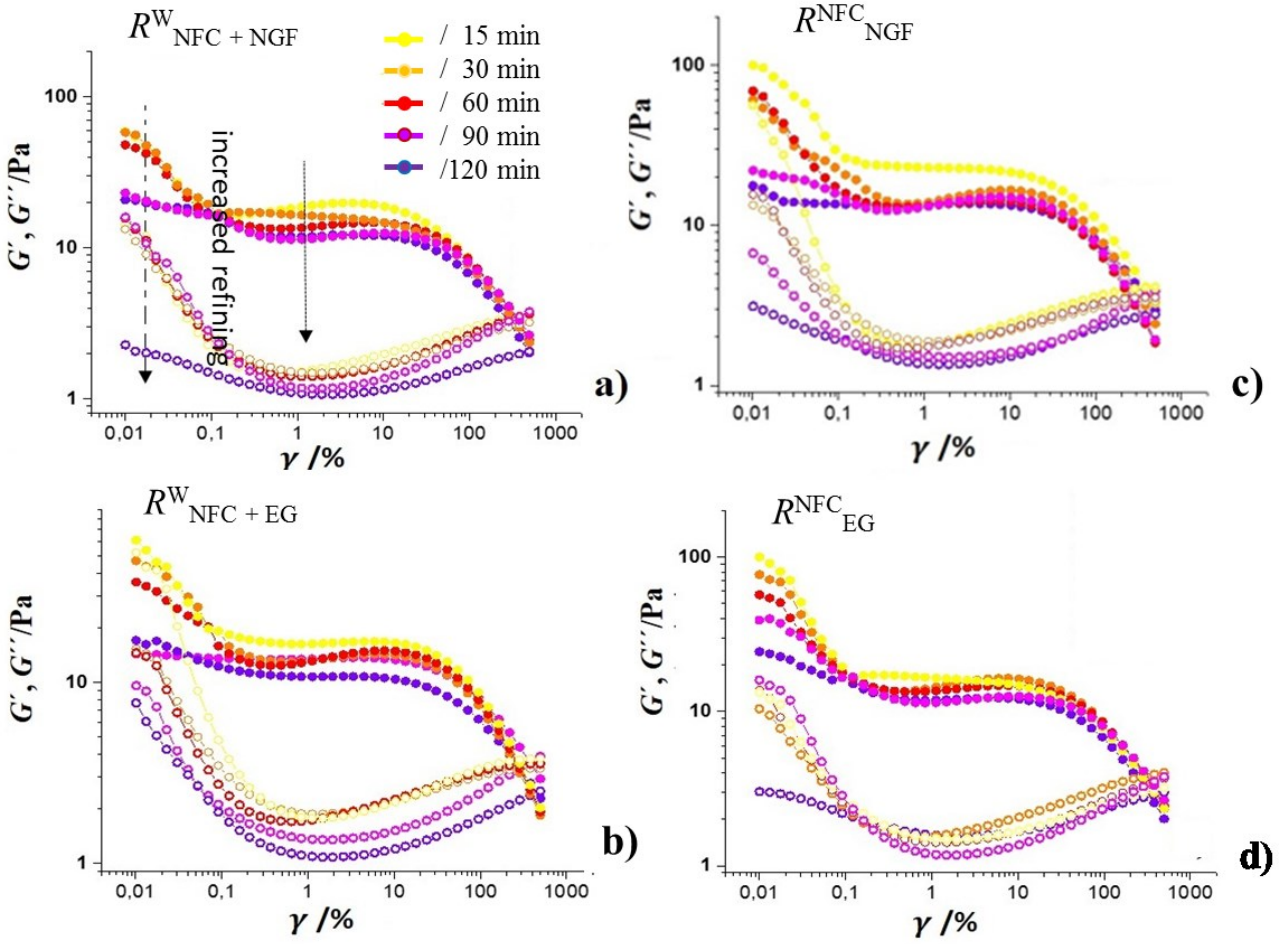

Fig. 5 Viscoelastic moduli G' (solid symbols) and G'' (open symbols) obtained from amplitude sweep tests where the strain span is from 0.01-500 % revealing the combined floc and gel-like graphene-NFC suspension structure: post processing mixed samples (a) $R^{W}_{NFC+NGF}$, (b) R^{W}_{NFC+EG}, and coprocessed samples (c) R^{NFC}_{NGF}, and (d) R^{NFC}_{EG}.

Table 4 Values of elastic (G') and loss moduli ([G'') at two different values of strain (γ = 0.01 % and 1.12 %), capturing the two-stage structure breakdown of loose flocs followed by stronger aggregates.

Refining time /min	$G'_{\gamma = 0.01\ \%}$ **/Pa**				$G'_{\gamma = 1.12\ \%}$ **/Pa**			
	$R^{W}_{NFC+NGF}$	R^{W}_{NFC+EG}	R^{NFC}_{NGF}	R^{NFC}_{EG}	$R^{W}_{NFC+NGF}$	R^{W}_{NFC+EG}	R^{NFC}_{NGF}	R^{NFC}_{EG}
15	98.23	92.12	132.23	103.23	32.94	28.69	36.44	34.32
30	84.78	71.34	102.53	99.12	24.91	21.44	29.41	28.52
60	69.56	59.45	79.12	75.23	17.25	14.57	23.57	22.13
90	58.09	51.34	66.23	62.12	13.13	11.37	19.37	18.52
120	37.76	32.07	42.23	39.34	10.52	9.23	14.84	12.75
	$G''_{\gamma = 0.01\ \%}$ **/Pa**				$G''_{\gamma = 1.12\ \%}$ **/Pa**			
	$R^{W}_{NFC+NGF}$	R^{W}_{NFC+EG}	R^{NFC}_{NGF}	R^{NFC}_{EG}	$R^{W}_{NFC+NGF}$	R^{W}_{NFC+EG}	R^{NFC}_{NGF}	R^{NFC}_{EG}
15	31.96	29.77	46.23	43.12	21.77	19.57	28.36	22.67
30	25.43	23.36	34.36	31.41	15.88	14.55	21.18	17.52
60	18.28	16.56	27.56	24.28	12.74	11.00	17.95	14.49
90	16.76	14.72	21.73	19.56	9.86	7.42	14.00	11.41

120	12.96	11.62	17.73	14.96	7.14	5.09	11.17	8.57

Interestingly, also in Table 4, the suspected increased coupling between NFC and graphene particles when the two are coprocessed is supported by comparatively higher structural strength and viscosity values, i.e. $\{G', G'' (R^{NFC}_{NGF})\} > \{G', G'' (R^{W}_{NFC+NGF})\}$ and $\{G', G'' (R^{NFC}_{EG}) > \{G', G'' (R^{W}_{NFC+EG})\}$, respectively. The somewhat greater ease of refining EG compared with NGF is also reflected in the lower moduli values, as was seen in the increased water retention behaviour for the coprocessed NFC-EG composite.

The elastic moduli ($G'$and G'') of all the NFC-graphene composite suspensions show similar response to increasing angular frequency (ω) under oscillation, Fig. 6, displaying initially weak structure breakdown, as was seen under low strain, Fig. 5, followed by high frequency vibration-induced elastic behaviour [40]. This observation clearly indicates that the stronger aggregation structure in the NFC medium becomes ever more more rigid under vibration, following a hardening response [43, 49, 51]. Fascinatingly, the greater the refining time, the weaker the initial static structure, as seen before in Fig. 5, but the greater the relative induced elastic hardening, seen as a cross-over from the lowest modulus value at low frequency to the highest or close to highest at high frequency [52, 59, 60]. This reveals that the effect is one of particle number; the more particles present, the greater is the elastic hardening. Such materials make useful vibration resistant materials, for example in buildings under earthquake conditions.

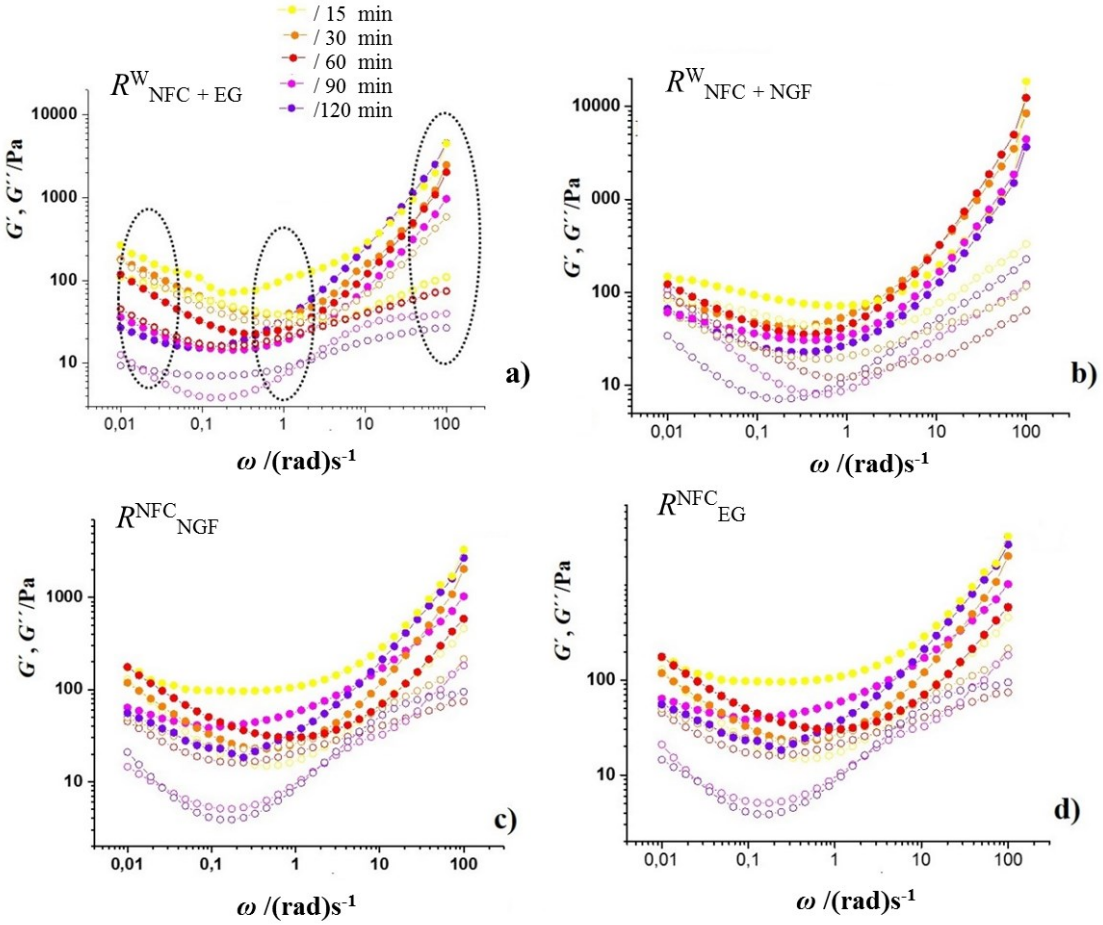

Fig. 6 Elastic moduli (G' and G'') dependence on angular frequency (ω) reveals the changing influence from weak floc interactions, which become broken down, to that of strong particle-particle interactions delivering a

vibration-induced hardening (ringed regions): post processing mixed samples (a) R^{W}_{NFC+EG}, (b) $R^{W}_{NFC+NGF}$, and coprocessed samples (c) R^{NFC}_{NGF}, (d) R^{NFC}_{EG}.

The shear thinning behaviour of graphene-NFC suspensions within the viscoelastic region under oscillation was traced using the complex viscosity (η^*) response to increased angular frequency (ω) under constant strain, as presented in Fig. 7. Shear thinning behaviour at low to intermediate angular frequency can be seen to change to dilatant behaviour at higher frequencies due to the presence of the strongly interacting aggregated graphene particles [3, 36, 41].

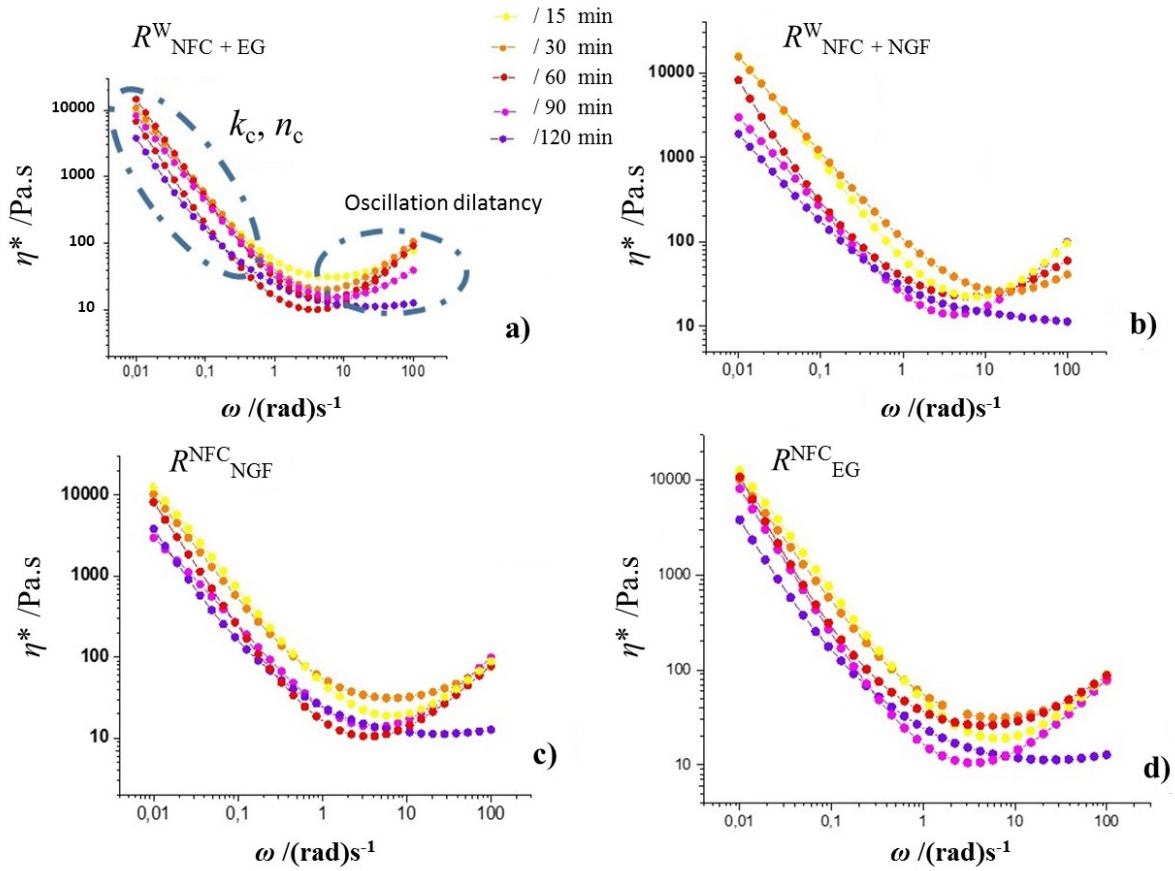

Fig. 7 Complex viscosity (η^*) response to increase of angular frequency ω = 0.01-100 (rad)s^{-1}, showing the Ostwald-deWaele complex viscosity thinning analogue parameters k_c and n_c, and the region of oscillation dilatancy: post processing mixed samples (a) R^{W}_{NFC+EG} (b) $R^{W}_{NFC+NGF}$, and coprocessed samples (c) R^{NFC}_{NGF}, (d) R^{NFC}_{EG}.

The thixotropic response is parameterised using the Ostwald-de Wael analogue expression under oscillation, Eq. 3, applied of the region ω = 0.01-10 (rad)s^{-1}, and the equivalent values of k_c and n_c are shown in Table 5 [10, 40, 41, 43]. It can be concluded that the smaller graphene particles produced from the EG starting graphite result in lower viscosity in NFC suspension, which is even more pronounced when the graphite is refined together with the NFC due to dispersive effect of the NFC during coprocessing, inducing also improved coupling with the applied shear.

Table 5 Complex viscosity (η^*) thixotropic response to increasing angular frequency fitted using an Ostwald-de Waele analogue power law at low-medium frequency providing a flow k_c and shear thinning coefficient n_c.

Refining time /min	$k_{c@\omega = 0.01\text{-}10\ (rad)\ s^{-1}}$				$n_{c@\omega = 0.01\text{-}10\ (rad)s^{-1}}$			
	$R^{W}_{NFC+NGF}$	R^{W}_{NFC+EG}	R^{NFC}_{NGF}	R^{NFC}_{EG}	$R^{W}_{NFC+NGF}$	R^{W}_{NFC+EG}	R^{NFC}_{NGF}	R^{NFC}_{EG}
15	98	85	112	106	0.21	0.18	0.22	0.22
30	88	67	109	105	0.17	0.16	0.24	0.21
60	65	56	84	74	0.15	0.11	0.19	0.18
90	44	38	62	56	0.11	0.08	0.15	0.14
120	37	23	49	43	0.09	0.07	0.11	0.11

3.2.2.2 Static versus dynamic stress analysis

Static yield stress (τ^0_s) was evaluated from the parallel plate strain amplitude response in the oscillatory measurements and defined as the maximum in static stress [τ_s] in response to increasing strain (γ), Fig. 8. This corresponds to the value of elastic modulus (G'), at critical strain, multiplied by the critical strain (γ_c), Eq. 5. The static yield stress (τ^0_s) is expected to be larger than the dynamic yield stress (τ^0_d), obtained from shearing conditions measured with vane geometry, and presented for the cases of graphene in water and graphene in surfactant solution in Fig. 4, as the structure is not broken prior to the application of strain [43, 50, 57].

Suspensions in which graphite has been refined with NFC have lower yield point (both static and dynamic), due to the less flocculation and more disperse state of the particles [43, 59]. Longer refining time leads to a decrease in particle size, and correspondingly results in smaller clusters of graphene aggregates for all graphene-NFC suspensions regardless of the processing route. This reduces the energy needing to bring the system into flow [54, 55].

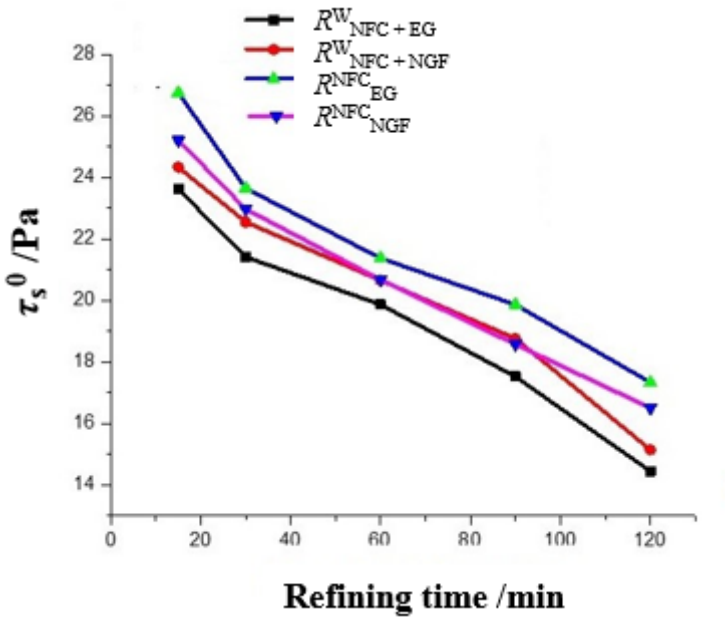

Fig. 8 Static yield stress under amplitude sweep test obtained as the maximum of stress dependence on strain, revealing the floc strength of the graphene-NFC suspensions.

The dynamic stress as a function of shear rate is complex, and perhaps displays the most promising information in respect to describing the material content in the graphene-NFC composite dispersions, Fig. 9, which can be drawn out only in the light of the rheological analyses described above [4, 8]. Dynamic stress is plotted for the shear rate range $\dot{\gamma}$ = 0.01 - 1 000 s^{-1}, and illustrates shear thinning followed by a minimum rising again rapidly to either a plateau of close to Newtonian behaviour or a slower shear thickening, and finally a strongly rheopectic/dilatant behaviour, reminiscent of filler in polymer dispersion [57, 58, 61]. These four concatenated domains of stress behaviour were fitted using the Herschel-Bulkley model, Eq. 1, delivering a dynamic yield point ($\tau_d{}^0{}_i$)at each domain concatenation point, together with a respective consistency index (k_i) and shear thinning coefficient (n_i) for each domain, providing insight into the effect of shear rate and refining time on the agglomeration of graphene in the NFC matrix.

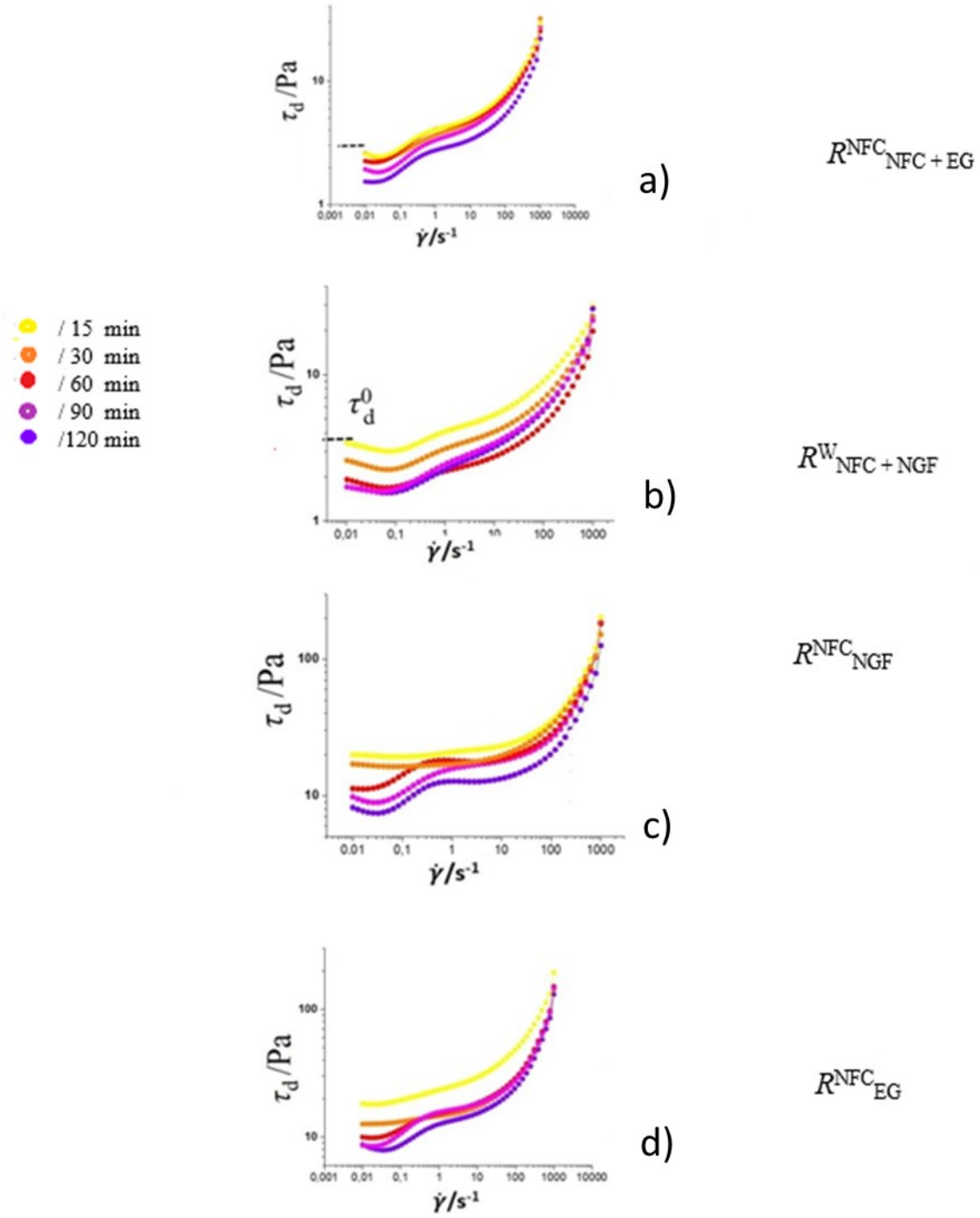

Fig. 9 Dynamic stress of graphene-NFC obtained using vane geometry, with four different intervals used for fitting curves following the Herschel-Bulkley power law expression, Eq. 1: (a) R^{W}_{NFC+EG}, (b) $R^{W}_{NFC+NGF}$, and coprocessed samples (c) R^{NFC}_{NGF}, and (d) R^{NFC}_{EG}.

The four shear rate domains were divided logarithmically into an ultralow shear region $\dot{\gamma}$ = 0.01 - 0.1 s^{-1}, a low shear region $\dot{\gamma}$ = 0.1 - 1 s^{-1}, an intermediate region $\dot{\gamma}$ = 1 - 10 s^{-1} and a high shear region $\dot{\gamma}$ = 10 - 1 000 s^{-1}. As we can see in Fig. 9, the benefit of studying the dynamic stress is that the method provides a large amount of data for curve fitting using the concatenated Herschel-Bulkley models. The ultralow shear region provides confirmation of the initially sheared floc and retained gel-like structure, the low shear and medium shear

indicate the breakdown and transition minimum of the structured state, and the short region of quasi steady state, respectively [52, 59]. Use of the stress data provides the real benefit of studying the high shear region in detail [42, 49]. Analysing this region will now allow us to interpret the primary aggregate structure of the various systems.

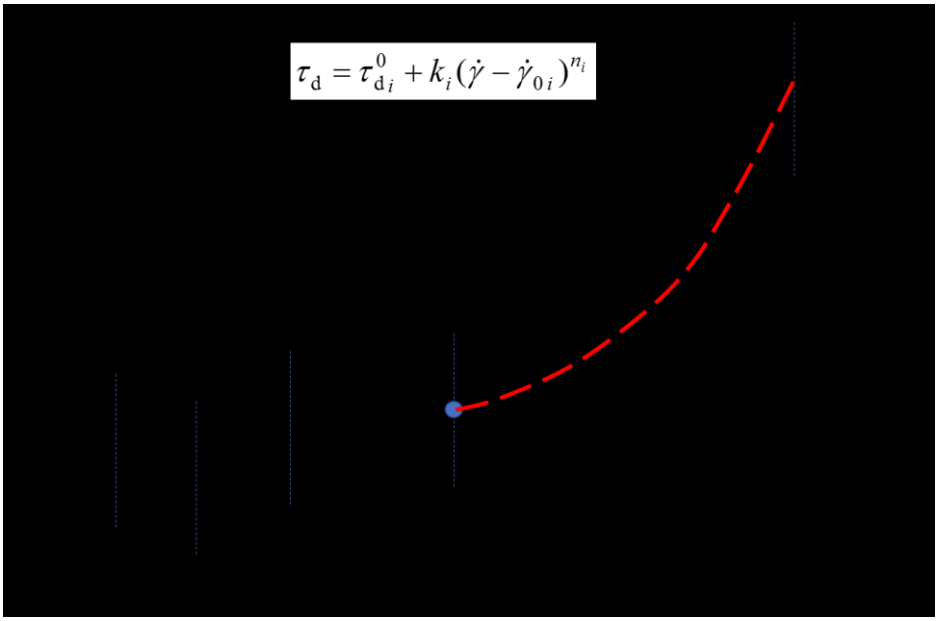

Fig. 10 The four regions of exponential change, showing the fourth characteristic behaviour of stress growth fitted using the Herschel-Bulkley expression.

By observing the Herschel-Bulkley concatenate dynamic yield stress $\tau_d{}^0{}_i$ for each domain together with the respective k_i and n_i (i = 1 to 4) values with respect to the processing conditions for the two graphene sources it is possible to correlate the nanofibrillar cellulose effect of dispersing seen as a decrease in flocculation and agglomeration [indices k_i] and increase in yield points (τ_{d0i}) of graphene-NFC coprocessed suspensions when smaller particles are present in the matrix throughout the shear rate range, as shown in Fig. 9 and summarised in Fig. 11. Refining time has a high impact on the agglomeration of graphene particles and creation of clusters of graphene within the nanocellulose matrix, which affects the energy that needs to be introduced bring the system into flow.

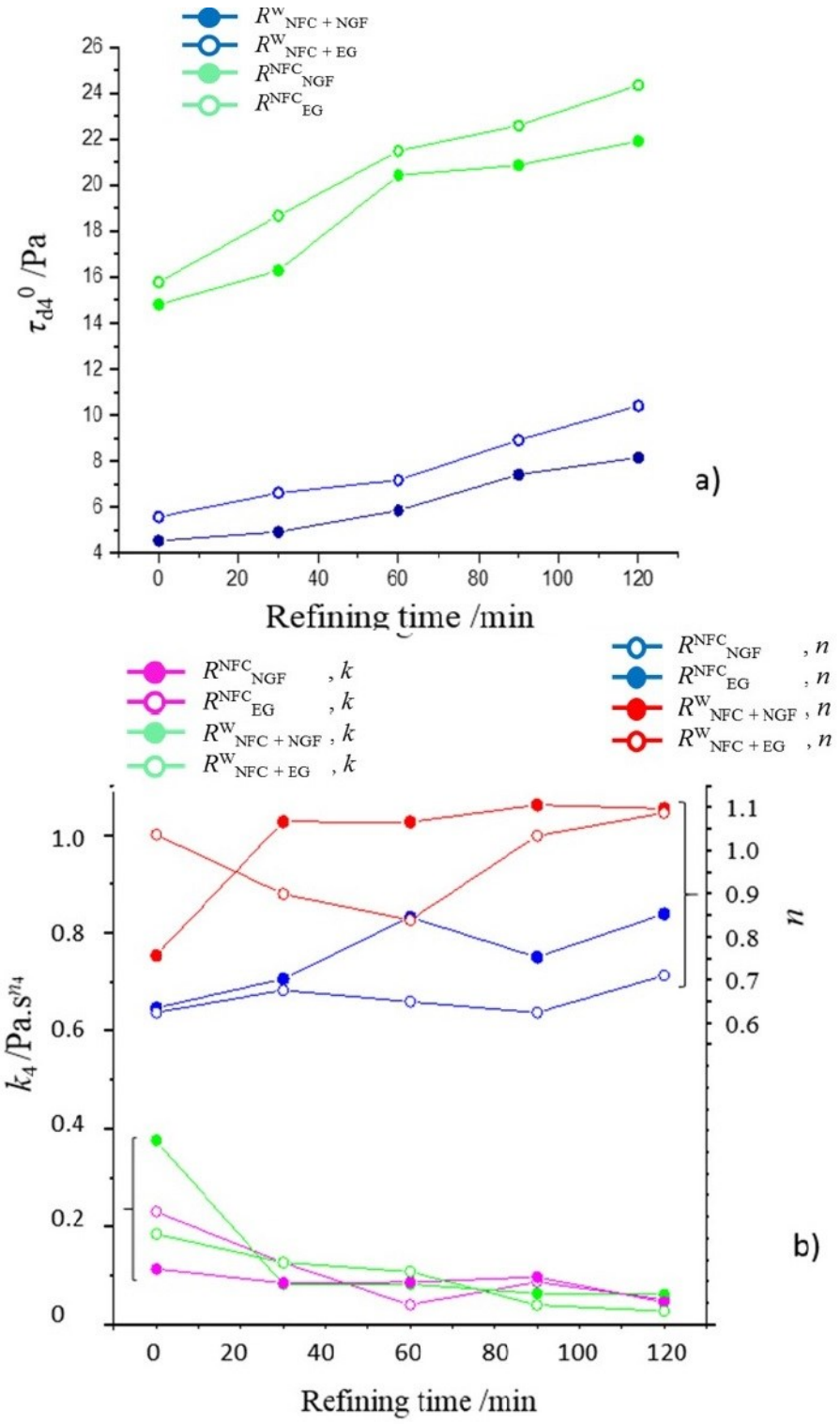

Fig. 11 Rheological parameters of (a) dynamic stress $\tau_d{}^0{}_{i=4}$, and (b) $k_{i=4}$ and $n_{i=4}$, showing the effect of increased dispersing when coprocessing with NFC and the clear trend of shear thinning followed by shear thickening as a function of shear rate.

3.2.2.2 Structure recovery

Refining time decreases structure recovery time, which was measured as the maximum reached in transient viscosity (η^{+}_{max}), after which a drastic decrease in transient viscosity is observed for all suspensions, Fig. 12. This combination of rheopectic behaviour, seen as transient viscosity increase at constant shear rate results in an overshoot peak upon eventual increase of shear rate, and then relates to the break-up of graphene clusters at high shear rates, as can be seen with the accompanying steady state curves, Fig. 12. Thus, we can expect a breakage of graphene aggregates within the NFC matrix after prolonged time, and this is revealed by the dramatic transient viscosity decrease and subsequent fast structure recovery [10, 13, 56].

Transient viscosity recovery in the third interval, is longest for the graphene derived from the NGF graphite flakes post-process mixed with separately processed NFC and displays the slowest rheopectic behaviour, which in turn decreases with increasing refining time, i.e. resulting from smaller agglomerates size. To trace structure recovery in the third interval, we reduce the values after it reaches the maximum, which occurs at different time intervals for each suspension, using the static starting state viscosity (η^{+}_{max}/η^{0}). For graphene-NFC suspensions derived from expanded graphite (EG), recovery after high shear is faster than for NGF-derived graphene, and correspondingly for those where graphene was ground with NFC, regardless of graphene origin.

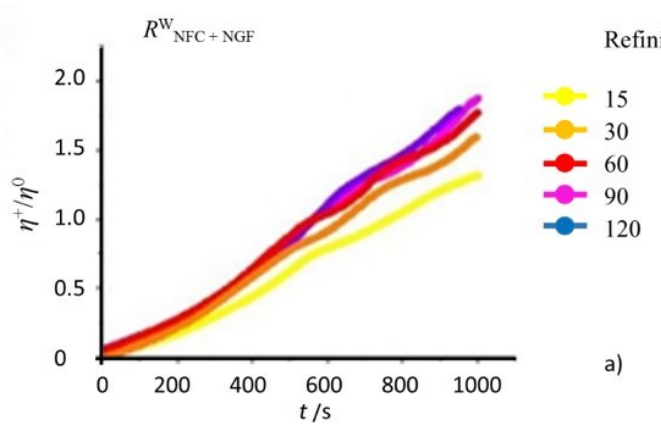
$R^{W}_{NFC + NGF}$
Refining time /s
15
30
60
90
120
η^+/η^0
t /s
a)

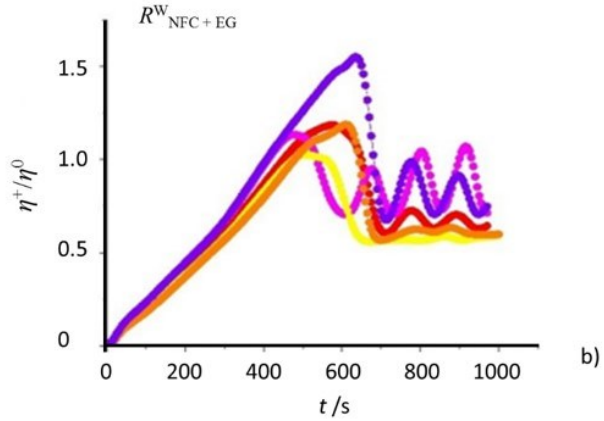
$R^{W}_{NFC + EG}$
η^+/η^0
t /s
b)

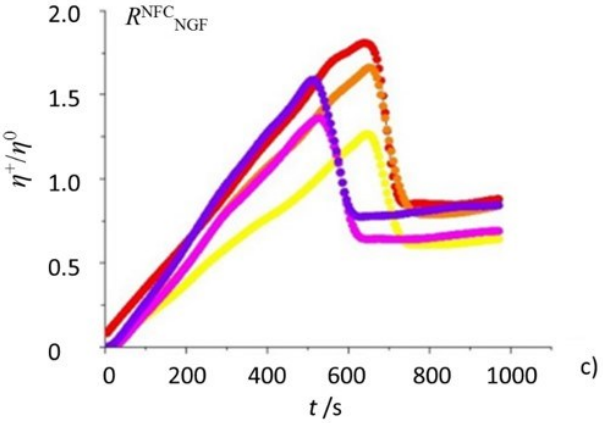
R^{NFC}_{NGF}
η^+/η^0
t /s
c)

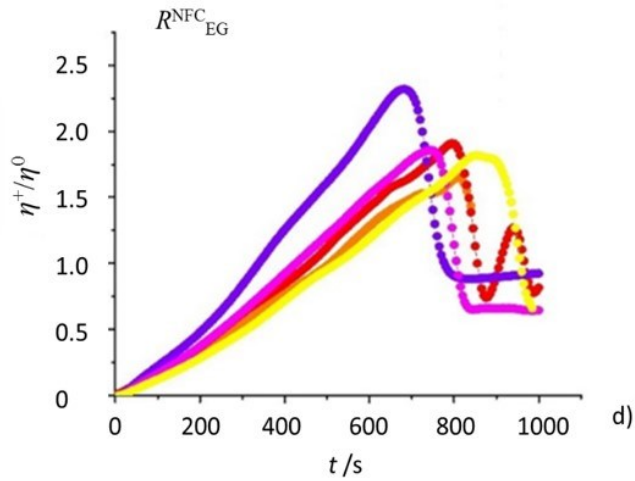
R^{NFC}_{EG}
η^+/η^0
t /s
d)

Fig. 12 Normalised transient viscosity [η^+/η^0] in third interval (low shear of 0.1 s^{-1}), measured after second interval of high shear (1 000 s^{-1}), to trace structure recovery in 3ITT recovery tests using vane geometry showing apparent dynamic viscosity up to the maximum overshoot values in the second, high shear, region: (a) $R^W_{NFC + NGF}$ displaying the greatest shear thinning, the most rapid rheopectic maximum and the fastest recovery.

3.3 Structure as viewed in the SEM

SEM images obtained from graphene in water suspensions upon processing at different refining times (for duration of refining of 30, 90 and 120 min) with water as medium reveal that few-layer graphene produced from expanded graphite (EG) suspensions have different morphological characteristics and reduced tendency to agglomerate than graphene formed from natural graphite flake suspensions (NGF), as presented in Fig.13, and that refining time leads to a decrease in agglomerate size [36].

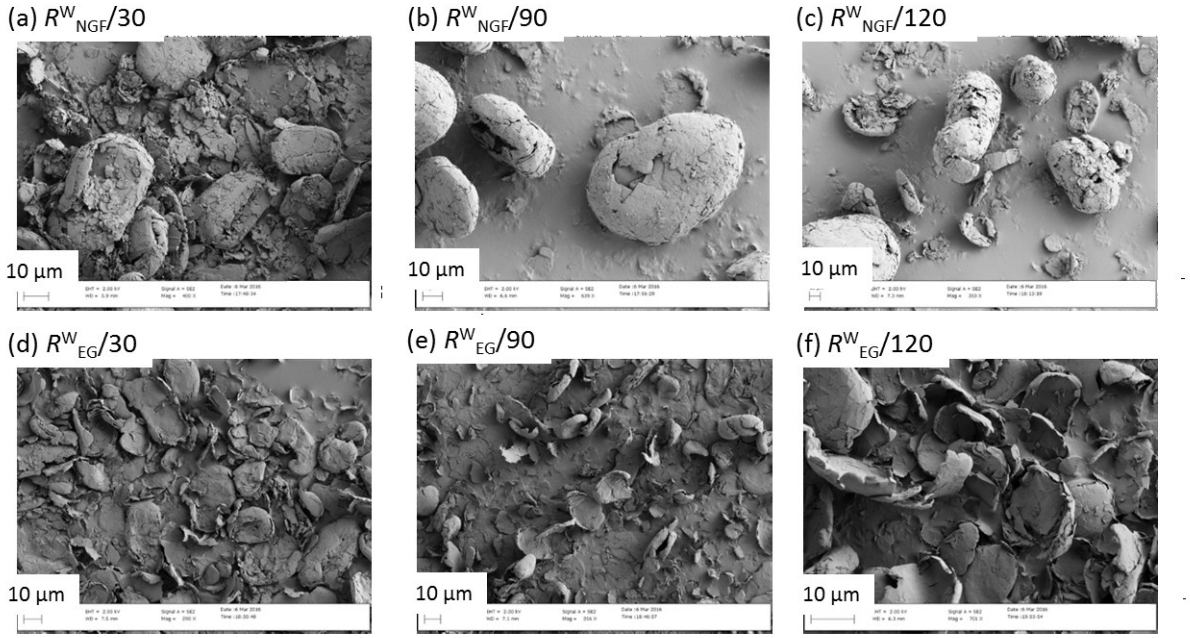

Fig. 13 SEM images revealing the influence of refining time, namely 30, 90 and 120 min, on agglomerate size and shape in two different sets of refined few layer graphene suspensions: (a), (b), (c) from NGF; (d), (f), €, (f) from EG.

When graphene is produced via refining together with nanocellulose suspension, it is much more uniformly distributed throughout the NFC suspension, which leads to more compact and less porous graphene platelets, Fig. 14, for both EG and NGF ground together with NFC [36, 58]. Refining time has an influence on the morphology of the platelets, as in the previous Fig. 13 with water only, but the result of more uniform and less aggregated agglomeration of the graphene particles coprocessed with NFC suspension demonstrates the universal dispersing power and increased hydrodynamic coupling with the fluid phase when including NFC [13, 36].

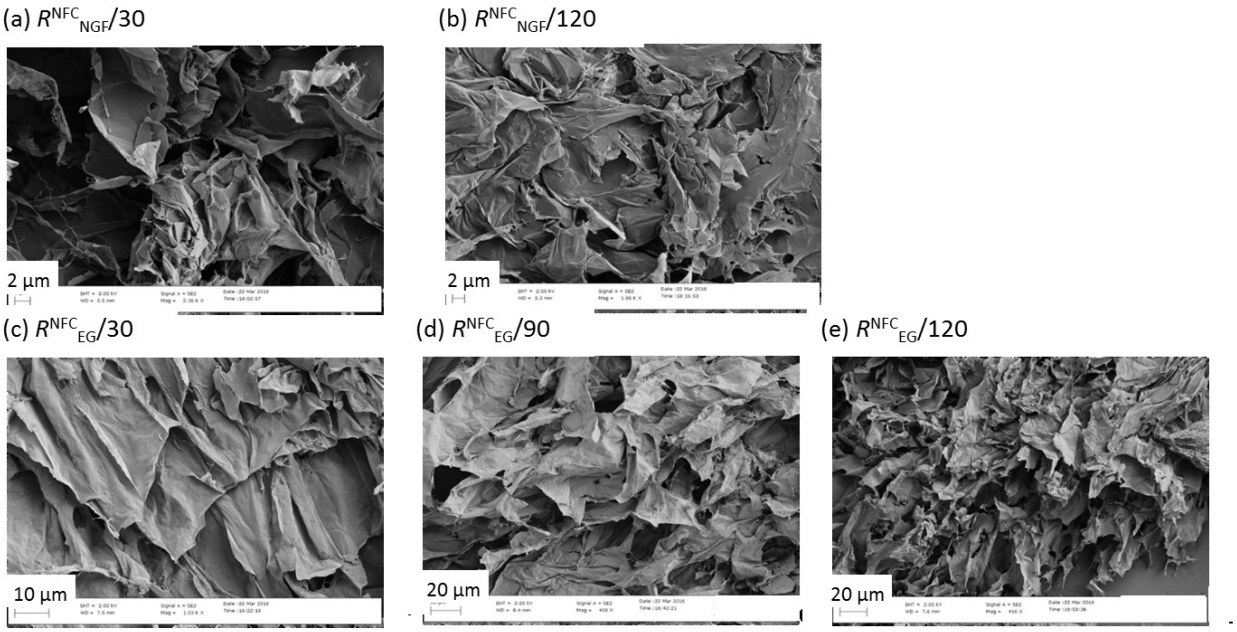

Fig. 14 SEM images showing the influence of coprocessing with NFC suspension on few layer graphene platelet morphology and size for the two graphite sources: (a) (b) NGF, and (c), (d), (e) EG, respectively, for the different refining times, 30, 90 and 120 min.

Contrasting Fig. 15 with Fig. 14 shows clearly the advantage of coprocessing with NFC versus simple mixing after processing. When graphite is processed separately from the NFC suspension, and only with the poorly coupled hydrodynamic effect of water, it retains much bigger agglomerates than when coprocessed simultaneously, and with further flocs amongst the post-added NFC fibrils creating the appearance of a more broken platelet structure [38]. Once again, as In Fig. 3, we see the greater uniformity of the product when using EG versus NGF, Fig. 15.

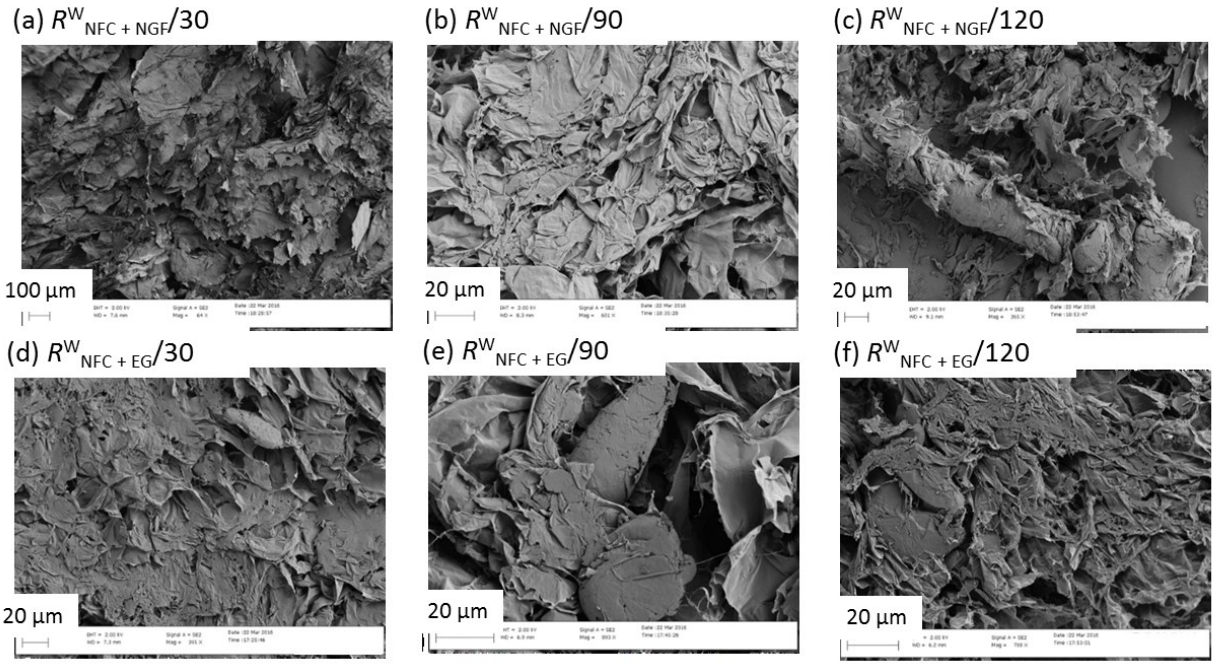

Fig. 15 SEM images presenting few layer graphene processed in water from the two types of graphite post-mixed with separately processed NFC: (a), (b), (c) NGF, and (d), (e), (f) EG: processing times 30, 90 and 120 min. Post addition of separately processed NFC fails to disperse the agglomerated graphene structure.

We can conclude from the SEM images, that the average agglomerate size of graphene suspensions decreases with refining time [10, 13]. The coprocessing with NFC is successful in dispersing graphene and enabling improved graphene platelet morphology. NFC used as a simple additive after refining the graphite, however, may be considered ineffective. The SEM visual assessment is supported by the dynamic laser light scattering particle size results, Fig. 16 and Table 5, and shows us by the inclusion of the results for coprocessing with surfactant (SC solution) that the surfactant behaves similarly to the coprocessing with NFC, but that post addition of NFC is confirmed to be virtually ineffective.

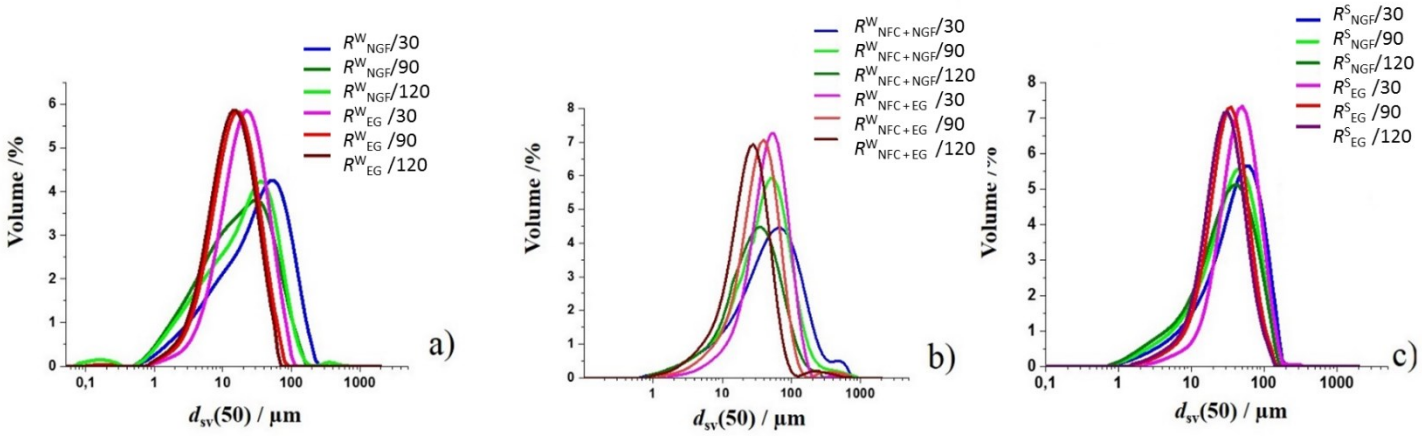

Fig. 16 Examples of the volume equivalent agglomerate particle size distribution as measured using light scattering of products derived from graphite refining into few layer graphene in (a) water alone, (b) post mixing with NFC and (c) coprocessing in surfactant solution (S).

Table 5 Median agglomerate size, d_{SV} (50), as measured by light scattering comparing water medium processing, post process mixed graphene with NFC, and processing in surfactant solution medium.

Sample	**Scattering volume equivalent** d_{SV} (50) / µm
R^W_{NGF} /30	40.16
R^W_{NGF} /90	32.36
R^W_{NGF} /120	28.85
R^W_{EG} /30	42.89
R^W_{EG} /90	29.81
R^W_{EG} /120	26.23
$R^W_{NFC+NGF}$ /30	47.56
$R^W_{NFC+NGF}$ /90	33.86
$R^W_{NFC+NGF}$ /120	32.49
R^W_{NFC+EG} /30	44.49
R^W_{NFC+EG} /90	32.51
R^W_{NFC+EG} /120	28.64
R^S_{NGF} /30	29.51
R^S_{NGF} /90	15.72

R^S_{NGF}	/120	18.84
R^S_{EG}	/30	19.18
R^S_{EG}	/90	14.00
R^S_{EG}	/120	12.71

Median agglomerate size is highly dependent on refining time, and decreases with increase in refining [38, 14]. Finer agglomerate size is observed for graphene processed with surfactant, R^S_{NGF} and R^S_{EG}. The agglomerate size of the correspondingly post process mixed graphene and NFC suspension is seen to be similar to that when processing with water alone, as was visualised in the SEM images.

4. Conclusions

Graphene particles were produced with different refining time in a high shear reactor with the adi or surfactants, water, and annocellulose. Various degrees of graphene platelet integrity depend upon the processing conditions and the optional adoption of surfactant to aid dispersion of the hydrophobic nanometre-thin carbon material. Previous material analyses have studied surface area, microscopical morphological analysis and related these to energy input and chemical environment. However, if such a process for producing few-layer graphene at significantly reduced costs under the environmentally friendly conditions proposed, avoiding potentially environmentally damaging chemistry is to become relevant on an industrial scale, it is important to develop quality control parameterisation that is respectively straightforward to apply. Such a sensitive analysis can be provided by parameterising the rheological response of aqueous suspension stress to shear rate as a function of product and micro nanofibrillated cellulose processing properties, including formulation and end-product target characteristics. In comparison to simple post process adding of materials together, it has been possible to establish a relationship between the coprocessing properties and the end-product suspension stress response to increasing shear rate.

References

1 Klemm D, Kramer F, Moritz S, Lindstrom T, Ankerfors M, Gray D, Dorris A [2011] Nanocelluloses: a new family of nature-based materials. Angew Chem Int Ed Engl 50:5438-5466

2 Moon RJ, Martini A, Nairn J, Simonsen J, Youngblood J [2011] Cellulose nanomaterials review: structure, properties and nanocomposites. Chem Soc Rev 40:3941-3994

3 Zimmermann T, Pöhler E, Geiger T [2004] Cellulose Fibrils for Polymer Reinforcement 6:754-761

4 Hubbe MA, Tayeb P, Joyce M, Tyagi P, Kehoe M, Dimic-Misic K, Pal L [2017] Rheology of Nanocellulose-rich Aqueous Suspensions: a Review. BioResources, 12[4], 9556-9661

5 Sehaqui H, Zhou Q, Berglund LA [2011] Nanostructured biocomposites of high toughness-a wood cellulose nanofiber network in ductile hydroxyethylcellulose matrix 7:7342-7350

6 Paakko M, Vapaavuori J, Silvennoinen R, Kosonen H, Ankerfors M, Lindstrom T, Berglund LA, Ikkala O [2008] Long and entangled native cellulose I nanofibers allow flexible aerogels and hierarchically porous templates for functionalities 4:2492-2499

7 Saito T, Kimura S, Nishiyama Y, Isogai A [2007] Cellulose Nanofibers Prepared by TEMPO-Mediated Oxidation of Native Cellulose 8:2485-2491

8 Iotti M, Gregersen O, Weiby, Moe S, Lenes M [2011] Rheological Studies of Microfibrillar Cellulose Water Dispersions. J Polym Environ 19[1]:137-145.

9 Fukuzumi H, Saito T, Iwata T, Kumamoto Y, Isogai A [2008] Transparent and High Gas Barrier Films of Cellulose Nanofibers Prepared by TEMPO-Mediated Oxidation. Biomacromolecules 10 [1]:162-165

10 Pääkkönen T, Dimic-Misic K, OrelmaH., Pönni R, Vuorinen T, Maloney T [2016] Effect of xylan in hardwood pulp on the reaction rate of TEMPO-mediated oxidation and the rheology of the final nanofibrillated cellulose gel. *Cellulose*, *23*[1], 277-293

11 Dimic-Misic K, Puisto A, Gane P, Nieminen K, Alava M, Paltakari J, Maloney T [2013a] The role of MFC/NFC swelling in the rheological behavior and dewatering of high consistency furnishes. Cellulose 20 [6]:2847-2861

12 Fall AB, Lindström SB, Sundman O, Ödberg L, Wagberg L [2011] Colloidal stability of aqueous nanofibrillated cellulose dispersions. Langmuir 27 [18]:11332-11338

13 Rantanen J, Dimic-Misic K, Kuusisto J, Maloney TC [2015] The effect of micro and nanofibrillated cellulose water uptake on high filler content composite paper properties and furnish dewatering. *Cellulose*, *22*[6], 4003-4015

14 Isogai A, Saito T, Fukuzumi H [2011] TEMPO-oxidized cellulose nanofibers 3:71-85

15 Lee C, Wei X, Kysar JW, Hone J [2008] Measurement of the Elastic Properties and Intrinsic Strength of Monolayer Graphene. Science 321:385-388

16 Dürkop T, Getty SA, Cobas E, Fuhrer MS [2004] Extraordinary Mobility in Semiconducting Carbon Nanotubes. Nano Lett 4:35-39

17 Istrate OM, Paton KR, Khan U, O'Neill A, Bell AP, Coleman JN [2014] Reinforcement in melt-processed polymer–graphene composites at extremely low graphene loading level. Carbon 78:243-249

18 Zhao X, Zhang Q, Chen D, Lu P [2010] Enhanced Mechanical Properties of Graphene-Based Poly[vinyl alcohol] Composites. Macromolecules 43:2357-2363

19 Lee JU, Yoon D, Kim H, Lee SW, Cheong H [2011] Thermal conductivity of suspended pristine graphene measured by Raman spectroscopy. Physical Review B, 83[8], 081419

20 Peigney A, Laurent C, Flahaut E, Bacsa RR, Rousset A [2001] Specific surface area of carbon nanotubes and bundles of carbon nanotubes. Carbon 39:507-514

21 Bolotin KI, Sikes KJ, Jiang Z, Klima M, Fudenberg G, Hone J, Kim P, Stormer HL [2008] Ultrahigh electron mobility in suspended graphene. Solid State Commun 146:351-355

22 Balandin AA, Ghosh S, Bao W, Calizo I, Teweldebrhan D, Miao F, Lau CN [2008] Superior Thermal Conductivity of Single-Layer Graphene. Nano Lett 8:902-907

23 Stoller MD, Park S, Zhu Y, An J, Ruoff RS [2008] Graphene-based ultracapacitors. Nano Lett 8:3498-3502

24 Zhu Y, Murali S, Stoller MD, Ganesh KJ, Cai W, Ferreira PJ, Pirkle A, Wallace RM, Cychosz KA, Thommes M, Su D, Stach EA, Ruoff RS [2011] Carbon-Based Supercapacitors Produced by Activation of Graphene. Science 332:1537-1541

25 Torrisi F, Hasan T, Wu W, Sun Z, Lombardo A, Kulmala TS, Hsieh GW, Jung S, Bonaccorso F, Paul PJ, Chu D, Ferrari AC [2012] Inkjet-printed graphene electronics. ACS Nano 6:2992-3006

26 Wang, Jie, Ran Ran, Jaka Sunarso, Chao Yin, Honggang Zou, Yi Feng, Xiaobao Li, Xu Zheng, and Jianfeng Yao [2017] Nanocellulose-assisted low-temperature synthesis and supercapacitor performance of reduced graphene oxide aerogels. Journal of Power Sources 347 [2017]: 259-269

27 Wang X, Zhi L, Mullen K [2008] Transparent, conductive graphene electrodes for dye-sensitized solar cells. Nano Lett 8:323-327

28 Keeley GP, O'Neill A, McEvoy N, Peltekis N, Coleman JN, Duesberg GS [2010] Electrochemical ascorbic acid sensor based on DMF-exfoliated graphene. J Mater Chem 20:7864-7869

29 Hu K, Kulkarni DD, Choi I, Tsukruk VV [2014] Graphene-polymer nanocomposites for structural and functional applications. Prog Polym Sci 39:1934-1972

30 Scheuermann GM, Rumi L, Steurer P, Bannwarth W, Mulhaupt R [2009] Palladium nanoparticles on graphite oxide and its functionalized graphene derivatives as highly active catalysts for the Suzuki-Miyaura coupling reaction. J Am Chem Soc 131:8262-8270

31 Gao C, Zhang S, Wang F, Wen B, Han C, Ding Y, Yang M [2014] Graphene Networks with Low Percolation Threshold in ABS Nanocomposites: Selective Localization and Electrical and Rheological Properties 6:12252-12260

32 Malho JM, Laaksonen P, Walther A, Ikkala O, Linder MB [2012] Facile method for stiff, tough, and strong nanocomposites by direct exfoliation of multilayered graphene into native nanocellulose matrix. Biomacromolecules 13:1093-1099

33 Li, Yuanyuan, Hongli Zhu, Fei Shen, Jiayu Wan, Steven Lacey, Zhiqiang Fang, Hongqi Dai, and Liangbing Hu [2015] "Nanocellulose as green dispersant for two-dimensional energy materials. Nano energy 13: 346-354.

34 Sasidharan A, Panchakarla LS, Chandran P, Menon D, Nair S, Rao CNR, Koyakutty M [2011] Differential nano-bio interactions and toxicity effects of pristine versus functionalized graphene. Nanoscale, 3[6], 2461-2464.

35 Carrasco PM, Montes S, García I, Borghei M, Jiang H, Odriozola I, Cabañero G, Ruiz V [2014] High-concentration aqueous dispersions of graphene produced by exfoliation of graphite using cellulose nanocrystals. Carbon 70:157-163. doi: http://dx.doi.org/10.1016/j.carbon.2013.12.086.

36 Phiri J, Gane P, Maloney TC[2017]. High-concentration shear-exfoliated colloidal dispersion of surfactant–polymer-stabilized few-layer graphene sheets. Journal of Materials Science, 52[13], 8321-8337

37 Hadadian M, Goharshadi EK, Youssefi A [2014] Electrical conductivity, thermal conductivity, and rheological properties of graphene oxide-based nanofluids. Journal of nanoparticle research, 16[12], 2788

38 Sun P, Kuga S, Wu M, Huang Y [2014] Exfoliation of graphite by dry ball milling with cellulose 21:2469-2478

39 Rahman R, Foster JT, Haque A [2013] Molecular dynamics simulation and characterization of graphene–cellulose nanocomposites. The Journal of Physical Chemistry A, 117[25], 5344-5353

40 Yang Y, Grulke EA, Zhang ZG, Wu G [2005] Rheological behavior of carbon nanotube and graphite nanoparticle dispersions. Journal of nanoscience and nanotechnology, 5[4], 571-579

41 Umerova S, Ragulya A, Coexistence of Rheopexy and Dilatancy in Polymer Suspensions filled with Ceramic Nanoparticles. Rheol: Editorial open access 2017, 1:2

42 Mohtaschemi M, Dimic-Misic K, Puisto A, Korhonen M, Maloney T, Paltakari J, Alava M [2014] Rheological characterization of fibrillated cellulose suspensions via bucket vane viscometer. Cellulose 21[3]:1305-1312

43 Dimic-Misic K, Maloney TC, Gane PAC [2015] Defining a strain-induced time constant for oriented low shear-induced structuring in high consistency MFC/NFC-filler composite suspensions. J. Appl. Poly. Sci. DOI: 101002/APP.42827

44 Mandal A, Chakrabarty D [2014] Studies on the mechanical, thermal, morphological and barrier properties of nanocomposites based on poly [vinyl alcohol] and nanocellulose from sugarcane bagasse. Journal of Industrial and Engineering Chemistry, 20[2], 462-473

45 Mehrali M, Sadeghinezhad E, Latibari ST, Kazi SN, Mehrali M, Zubir MNBM, Metselaar HSC [2014] Investigation of thermal conductivity and rheological properties of nanofluids containing graphene nanoplatelets. Nanoscale research letters, 9[1], p.15

46 Tseng WJ, Wu CH [2002] Aggregation, rheology and electrophoretic packing structure of aqueous Al_2O_3 nanoparticle suspensions. Acta materialia, 50[15], 3757-3766

47 Shih WY, Shih WH., Aksay I A [1999] Elastic and yield behavior of strongly flocculated colloids. Journal of the American Ceramic Society 82[3]: 616-624

48 Yang MC, Scriven LE, Macosko C W [1986] Some rheological measurements on magnetic iron oxide suspensions in silicone oil. Journal of Rheology 30[5]: 1015-1029

49 Walls HJ, Caines SB, Sanchez AM, Khan SA [2003] Yield stress and wall slip phenomena in colloidal silica gels. Journal of Rheology 47[4]: 847-868

50 Barnes HA, Ngyen QD [2001] Rotating vane rheometry-a review. J. Non-Newtonian Fluid Mech. 98 [1], 1-14

51 Mewis J, Wagner NJ [2009] Thixotropy. Adv Colloid Interface Sci 147:214-227

52 Dimic-Misic K, Maloney T, Gane P [2018] Effect of fibril length, aspect ratio and surface charge on ultralow shear-induced structuring in micro and nanofibrillated cellulose aqueous suspensions. Cellulose, 25[1], 117-136

53 Dimic-Misic K, Maloney T, Liu G, Gane P [2017] Micro nanofibrillated cellulose [MNFC] gel dewatering induced at ultralow-shear in presence of added colloidally-unstable particles. Cellulose, 24[3], 1463-1481

54 Kavan L, Yum JH, Gratzel M [2011] Optically transparent cathode for dye-sensitized solar cells based on graphene nanoplatelets. ACS Nano 5:165-172

55 Divoux T, Barentin C, Manneville S [2011] From stress-induced fluidization processes to Herschel-Bulkley behaviour in simple yield stress fluids. Soft Matter 7[18]: 8409-8418

56 Puisto A, Illa X, Mohtaschemi M, Alava M [2012a] Modeling the viscosity and aggregation of suspensions of highly anisotropic nanoparticles. Eur Phys J E 35[1]:1-7

57 Deka A, Dey N [2013] Rheological studies of two component high build epoxy and polyurethane based high performance coatings. J Coat Technol Res 10 [3]:305-315

58 Sha X, Yu K, Cao H, Qian K [2013] Shear thickening behavior of nanoparticle suspensions with carbon nanofillers. Journal of nanoparticle research, 15[7], 1816

59 Buscall R, Mills P, Stewart R, Sutton D, White L, Yates G [1987] The rheology of strongly-flocculated suspensions. J. Non-Newtonian Fluid Mech. 24 [2]: 183-202

60 Dimic-Misic K, Nieminen K, Gane P, Maloney T, Sixta H, Paltakari J [2014] Deriving a process viscosity for complex particulate nanofibrillar cellulose gel-containing suspensions. Appl. Rheol 24:35616-35625

61 Roussel N, Lanos C [2004] Particle fluid separation in shear flow of dense suspensions: experimental measurements on squeezed clay pastes. Appl. Rheol. 14 256.

62 Dimic-Misic K, Salo T, Paltakari J, Gane P [2014] Comparing the rheological properties of novel nanofibrillar cellulose-formulated pigment coating colours with those using traditional thickener. Nord. Pulp. Pap. J .29 253

63 Dang LN, Seppälä J [2015] Electrically conductive nanocellulose/graphene composites exhibiting improved mechanical properties in high-moisture condition. Cellulose, 22[3], pp.1799-1812